The Region-specific Segregation and Catalytic Activity of Gold-silver Nanoparticles (Electronic Supplementary Information)

Xiang He,* Sheng-En Zhang, Feng Cheng, and Zhao-Xu Chen*

E-mail: xhe@niglas.ac.cn; zxchen@nju.edu.cn

Coordination-averaged atomic energies

In our lattice model, the total energy of the nanoparticle is the sum of all interatomic interactions of the nearest neighboring atoms pair (i, j):

$$E = \sum_{(i,j)} I_i^n + I_j^m, \tag{1}$$

where I_i^n and I_j^m are the so-called coordination-dependent atomic energies of the atom i (n-fold coordinated) and its neighboring atom j (m-fold coordinated). For monometallic bulk, I^z is defined as

$$I^z = \frac{E_0 - E_{coh}}{z}, \tag{2}$$

where E_0 is the energy of an isolated metal atom and E_{coh} is the cohesive energy of the z-fold coordinated bulk. It is easy to verify Eq. 1 from Eq. S2 and the definition of E_{coh}. To apply Eq. 1 in alloy nanoparticles such as the bimetallic bulk composed of metal A and B, the interatomic interaction between the two metal types should be known. For equimolar

bimetallic bulk AB, the cohesive energy is defined as

$$E_{coh}^{AB} = \frac{E_0^A + E_0^B}{2} - \frac{E}{2N},$$

(3)

where $2N$ denotes the total number of atoms in the bulk unit cell. Thus,

$$E = \left(\frac{E_0^A - E_{coh}^{AB}}{2} + \frac{E_0^B - E_{coh}^{AB}}{2}\right) \cdot 2N$$

(4)

To calculate the Au-Ag interaction, we calculated the E_{coh} of Au, Ag and AuAg bulks in the diamond phase (DIA), simple cubic phase (SC) and body centered cubic (BCC) phase by the density functional theory (DFT) PBE functional method. In these phases, there exist only Au-Ag neighboring pairs in the 1:1 alloy as demonstrated in Fig. S1.
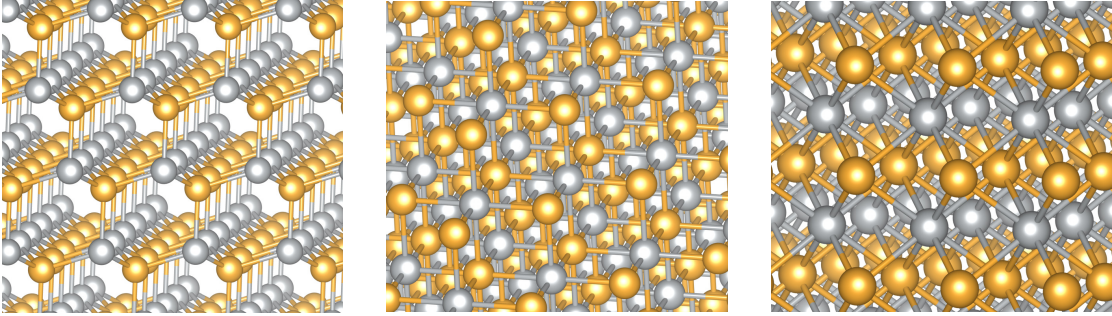

Figure S1: The diamond, simple cubic (NaCl) and body centered cubic structures of AuAg alloy.

Table S1: The E_{coh} of Au, Ag and alloy bulk

Phase	Au	Ag	AuAg
DIA	2.32	1.73	2.13
SC	2.84	2.18	2.54
BCC	3.01	2.49	2.79

The DFT results are listed in Table S1. It is worth noting that the E_{coh}^{AuAg} is very close

to the half of the sum of E_{coh}^{Au} and E_{coh}^{Ag}. In such case, Eq. 4 can be approximatelly cast into

$$
\begin{aligned}
E &= (\frac{E_0^{Au} + E_0^{Ag}}{2} - \frac{E_{coh}^{Au} + E_{coh}^{Ag}}{2}) \cdot 2N \\
&= (E_0^{Au} - E_{coh}^{Au} + E_0^{Ag} - E_{coh}^{Ag}) \cdot N \\
&= (I_{Au}^z + I_{Ag}^z) \cdot z \cdot N \\
&= \sum_{Au-Ag} I_{Au}^z + I_{Ag}^z
\end{aligned}
\tag{5}
$$

with the definition of I^z in Eq. S2. Hence, the interaction between the neighboring Au and Ag atoms is $I_{Au}^z + I_{Ag}^z$. Though Eq. 5 is a special case of Eq. 4 for the Au-Ag system, it simplifies the calculation of interatomic interaction between Au and Ag atoms.

The calculation of I_{Ag}^z

From Eqs. S2 and 5, it is clear that the accuracy of I^z depends on the adopted cohesive energies. We prefer physically measured energies in the calculations of I^z. However not all cohesive energies of different bulk phases are available. In this study, I_{Ag}^z is derived from various physical energies in a similar procedure of calculating I_{Au}^z[1] which is outlined as follows.

E_{coh}^{12} is known as 2.95 eV for the face-centered cubic (FCC) silver.[2] E_{coh}^1 is 0.82 eV from the dissociation energy of Ag_2.[3] The cohesive energies of other silver bulks without physical measurements, such as E_{coh}^4 of 1.20 eV in DIA phase, E_{coh}^6 of 2.24 eV in SC phase and E_{coh}^8 of 2.95 eV in BCC phase, are taken from KIM database of simulations based on effective medium theory (EMT) model (KIM ID: MO_118428466217_002).[4] It should be mentioned here that depending on the pseudopotential, the DFT calculations either underestimate or overestimate the cohesive energies. Therefor, we adopt E_{coh} from the literature results of EMT model which aims to fit the physical properties of bulks. In fact, the calculated cohesive energy of FCC silver bulk by the EMT model is 2.96 eV, which is very close to the

experimental result.

With a initial guess of E_0, I^{12}, I^8, I^6, I^4 and I^1 can be calculated by Eq. S2. Then all I^z are fitted by Eq. 6 as in Ref. 1.

$$I^z = A \cdot z^{-1/3} + B \cdot z^{-2/3} \tag{6}$$

Another physical measurement to correct the calculated I^z, the energy of removing one atom from the FCC bulk is used, which is just the sum of E_{coh}^{12} and the formation energy of vacancy E_{vac}^f. The latter was measured to be 0.89 eV.[5] In our model, this energy can be expressed as

$$E_{coh}^{12} + E_{vac}^f = E_0 + 11I^{11} \times 12 - 12I^{12} \times 13 \tag{7}$$

Since the l.h.s of Eq. 7 is determined by experimental values, an new E_0 can be calculated with I^{12} and I^{11} fitted by Eq. 6. The calculation process is repeated until E_0 is converged. Such that E_0 and I^z are iterative solutions to Eqs. S2, 6 and 7. The calculation results are present in Table S2 with I_{Au}^z.

Table S2: The coordination-averaged energies of Au and Ag atoms

z	I_{Au}^z	I_{Ag}^z	z	I_{Au}^z	I_{Ag}^z
E_{atom} *	-2.99	-2.72			
1	-4.13	-3.54	7	-0.91	-0.78
2	-2.46	-2.11	8	-0.81	-0.70
3	-1.80	-1.55	9	-0.74	-0.63
4	-1.44	-1.23	10	-0.67	-0.58
5	-1.20	-1.03	11	-0.62	-0.53
6	-1.03	-0.89	12	-0.57	-0.49

* E_{atom} is the energy of isolated atom in Ref. 1.

To verify the reliability and accuracy of low-coordinated I_{Ag}^z as well as Eq. 5, we calculated the energy of the single Ag adatom desorbing from the Au(111) surface. The energy is 2.05 eV calculated by our model, which is in nice agreement with DFT (PBE functional) calculated 2.10 eV and much better than the very recent embedded-atom method (EAM) result 2.35 eV.[6]

The calculation of I_{Pt}^z and I_{Pd}^z

Though the dissociation energy D_0 of dimer and E_{vac}^f are required, the calculation of I^z mainly depends on the cohesive energies of different bulk phases. If all energies involved in the calculation are physically measured, the I^z is non-empirical. In Table S3, we collect the related energy parameters of Pt and Pd to calculate I_{Pt}^z and I_{Pd}^z. The E_{coh}^{BCC}, E_{coh}^{SC} and E_{coh}^{DIA}

Table S3: The E_{coh} of Pt and Pd bulk, D_0 of Pt_2 and Pd_2 and E_{vac}^f of FCC Pt and Pd

	E_{coh}^{FCC}	E_{coh}^{BCC}	E_{coh}^{SC}	E_{coh}^{DIA}	D_0	E_{vac}^f
Pt	5.84	5.79	5.39	4.97	3.14[7]	1.15[8]
Pd	3.89	3.85	-	3.13	1.03[9]	1.70[10]

are also adopted from the EMT simulation results in KIM database. The E_{coh}^{FCC} are from experimental results, which are quite close to the EMT results. The derived I_{Pt}^z and I_{Pd}^z are listed in Table S4.

Table S4: The coordination-averaged energies of Pt and Pd

z	I_{Pt}^z	I_{Pd}^z	z	I_{Pt}^z	I_{Pd}^z
E_{atom}	-7.33	-5.56			
1	-8.92	-6.09	7	-1.86	-1.33
2	-5.24	-3.62	8	-1.66	-1.19
3	-3.80	-2.65	9	-1.49	-1.08
4	-3.00	-2.11	10	-1.35	-0.98
5	-2.49	-1.76	11	-1.24	-0.90
6	-2.13	-1.52	12	-1.14	-0.84

Model and MC simulations

Previous studies demonstrate that the metallic nanoparticle with faceted structure are stable and Ringe et al. found that the equilibrium shape of Au-Ag alloy nanoparticles approaches the traditional Wulff construction.[11–13] Therefore, the nanoparticles are modeled in a rigid three-dimensional lattice with Wulff structures and each lattice site is either unoccupied or occupied by one metallic atom.[14] In the MC simulations, the metallic atom tries to

exchange with the nearest neighbor atom in each *MC step*. In one *MC cycle*, all atoms of the nanoparticle have attempted to exchange sequentially. The exchange is accepted if the probability of acceptance, p, is larger than a random number between 0 and 1.[15] In our study, the p under temperature T is calculate by

$$p = \frac{1}{1 + e^{\Delta E / k_B T}}, \tag{8}$$

where ΔE is the energy change of the exchange and k_B is the Boltzmann constant. Fig. S2 shows the structures of 4.5 nm alloy nanoparticles at 300 K after simulated for 10^5 MC cycles.
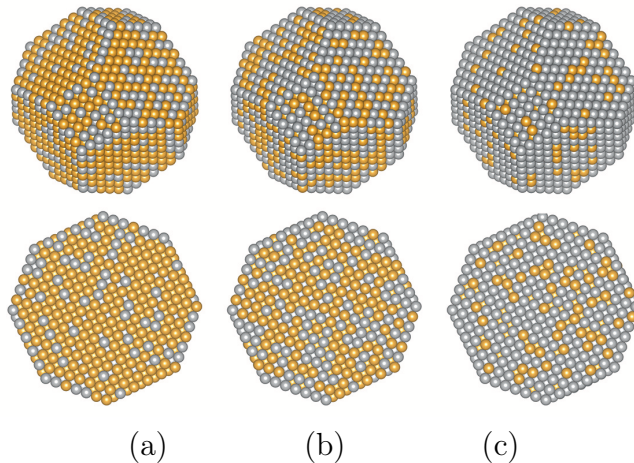

(a)   (b)   (c)

Figure S2: The structures and cross-sections of 4.5 nm alloy nanoparticles at 300 K. (a) $Ag_{0.25}Au_{0.75}$, (b) $Ag_{0.5}Au_{0.5}$, and (c) $Ag_{0.75}Au_{0.25}$. Gold and silver atoms are in yellow and gray respectively.

Temperature-dependent P_{type}^{Ag}

Table S5: P_{type}^{Ag} of 2.6 nm Ag_xAu_{1-x}

| | P_{edge}^{Ag} | | | P_{face}^{Ag} | | | P_{core}^{Ag} | |
x	100 K	300 K	600 K	100 K	300 K	600 K	100 K	300 K	600 K
0.10	0.52	0.27	0.18	0.04	0.09	0.10	0.01	0.05	0.07
0.15	0.71	0.37	0.26	0.08	0.15	0.15	0.02	0.08	0.11
0.25	0.90	0.53	0.40	0.24	0.25	0.26	0.06	0.16	0.20
0.33	0.95	0.64	0.50	0.39	0.35	0.35	0.11	0.23	0.27
0.50	0.98	0.78	0.65	0.66	0.53	0.51	0.26	0.40	0.45

Table S6: P_{type}^{Ag} of 3.7 nm Ag_xAu_{1-x}

| | P_{edge}^{Ag} | | | P_{face}^{Ag} | | | P_{core}^{Ag} | |
x	100 K	300 K	600 K	100 K	300 K	600 K	100 K	300 K	600 K
0.10	0.70	0.30	0.19	0.10	0.12	0.11	0.02	0.07	0.08
0.15	0.84	0.40	0.27	0.19	0.18	0.17	0.04	0.10	0.13
0.25	0.94	0.56	0.42	0.38	0.30	0.28	0.11	0.19	0.22
0.33	0.97	0.66	0.51	0.52	0.39	0.37	0.17	0.27	0.30
0.50	0.99	0.79	0.66	0.73	0.56	0.53	0.34	0.43	0.47

Table S7: P_{type}^{Ag} of 4.5 nm Ag_xAu_{1-x}

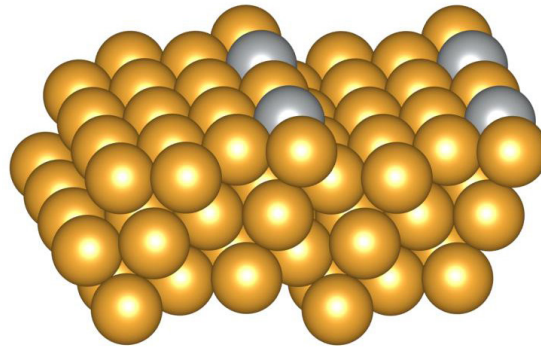| | P_{edge}^{Ag} | | | P_{face}^{Ag} | | | P_{core}^{Ag} | |
x	100 K	300 K	600 K	100 K	300 K	600 K	100 K	300 K	600 K
0.10	0.77	0.31	0.20	0.14	0.13	0.12	0.03	0.07	0.09
0.15	0.87	0.41	0.28	0.24	0.19	0.18	0.06	0.11	0.13
0.25	0.95	0.57	0.42	0.43	0.31	0.29	0.12	0.20	0.22
0.33	0.97	0.67	0.52	0.57	0.41	0.38	0.20	0.28	0.30
0.50	0.99	0.80	0.66	0.76	0.58	0.54	0.37	0.45	0.47

Stepped alloy surfaces

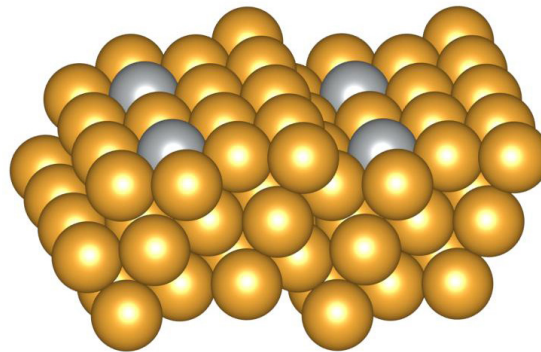Figure S3: The step edge on the surface is composed of equimolar Au and Ag atom.

Figure S4: The Ag atoms are doped on the terrace.

References

(1) He, X.; Cheng, F.; Chen, Z.-X. *Sci. Rep.* **2016**, *6*, 33128.

(2) Kambe, K. *Phys. Rev.* **1955**, *99*, 419–422.

(3) Ran, Q.; Schmude, R. W.; Gingerich, K. A.; Wilhite, D. W.; Kingcade, J. E. *J. Phys. Chem.* **1993**, *97*, 8535–8540.

(4) Tadmor, E. B.; Elliott, R. S.; Sethna, J. P.; Miller, R. E.; Becker, C. A. Knowledgebase of Interatomic Models (KIM). 2011; `https://openkim.org`.

(5) McGervey, J. D.; Triftshäuser, W. *Phys. Lett. A* **1973**, *44*, 53–54.

(6) Kotri, A.; El koraychy, E.; Mazroui, M.; Boughaleb, Y. *Surf. Interface Anal.* **2017**, *49*, 705–711, SIA-16-0392.R1.

(7) Taylor, S.; Lemire, G. W.; Hamrick, Y. M.; Fu, Z.; Morse, M. D. *J. Chem. Phys.* **1988**, *89*, 5517–5523.

(8) Emrick, R. M. *J. Phys. F: Metal Physics* **1982**, *12*, 1327.

(9) Shim, I.; Gingerich, K. A. *J. Chem. Phys.* **1984**, *80*, 5107–5119.

(10) Mattsson, T. R.; Mattsson, A. E. *Phys. Rev. B* **2002**, *66*, 214110.

(11) Baletto, F.; Ferrando, R.; Fortunelli, A.; Montalenti, F.; Mottet, C. *J. Chem. Phys.* **2002**, *116*, 3856–3863.

(12) Baletto, F.; Ferrando, R. *Rev. Mod. Phys.* **2005**, *77*, 371–423.

(13) Ringe, E.; Van Duyne, R. P.; Marks, L. D. *Nano Lett.* **2011**, *11*, 3399–3403.

(14) Wulff, G. *Z. Kristallogr. Miner.* **1901**, *34*, 449–530.

(15) He, X.; Huang, Y.; Chen, Z.-X. *Phys. Chem. Chem. Phys.* **2011**, *13*, 107–109.